Complete Thermodynamic and Kinetic Characterization of the Isomer-Specific Interaction between Pin1-WW Domain and the Amyloid Precursor Protein Cytoplasmic Tail Phosphorylated at Thr668

Soumya De,[†,#] Alexander I. Greenwood,[†] Monique J. Rogals,[†] Evgenii L. Kovrigin,[‡] Kun Ping Lu,[§] and Linda K. Nicholson*,[†]

[†]Department of Molecular Biology and Genetics, Cornell University, Ithaca, New York 14853, United States
[‡]Department of Chemistry, Marquette University, Milwaukee, Wisconsin 53201, United States
[§]Cancer Biology Program and Biology of Aging Program, Department of Medicine, Beth Israel Deaconess Medical Center, Harvard Medical School, Boston, Massachusetts 02215, United States

S *Supporting Information*

ABSTRACT: Peptidyl prolyl *cis*−*trans* isomerization acts as an effective molecular timer that plays significant roles in biological and pathological processes. Enzymes such as Pin1 catalyze *cis*−*trans* isomerization, accelerating the otherwise slow isomerization rate into time scales relevant for cellular signaling. Here we have combined NMR line shape analysis, fluorescence spectroscopy, and isothermal titration calorimetry to determine the kinetic and thermodynamic parameters

describing the *trans*-specific interaction between the binding domain of Pin1 (WW domain) and a key *cis*−*trans* molecular switch in the amyloid precursor protein cytoplasmic tail. A three-state model, in which the *cis*−*trans* isomerization equilibrium is coupled to the binding equilibrium through the *trans* isomer, was found to fit the data well. The *trans* isomer binds the WW domain with ~22 μM affinity via very fast association (approaching the diffusion limit) and dissociation rates. The common structural and electrostatic characteristics of Pin1 substrates, which contain a phosphorylated serine/threonine-proline motif, suggest that very rapid binding kinetics are a general feature of Pin1 interactions with other substrates. The fast binding kinetics of the WW domain allows rapid response of Pin1 to the dynamic events of phosphorylation and dephosphorylation in the cell that alter the relative populations of diverse Pin1 substrates. Furthermore, our results also highlight the vastly different rates at which slow uncatalyzed *cis*−*trans* isomerization and fast isomer-specific binding events occur. These results, along with the experimental methods presented herein, should guide future experiments aimed at the thermodynamic and kinetic characterization of *cis*−*trans* molecular switches and isomer-specific interactions involved in various biological processes.
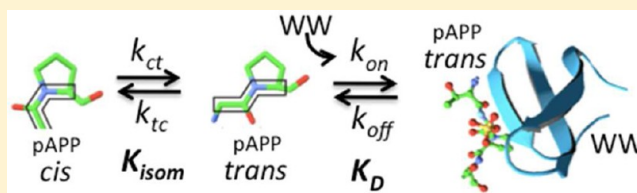
Pin1 is a peptidyl prolyl *cis*−*trans* isomerase (PPIase) enzyme that catalyzes the intrinsically slow *cis*−*trans* isomerization of the peptide bond in certain phosphorylated serine/threonine-proline (pS/T-P) motifs.[1,2] Through its interaction with specific substrates, Pin1 plays vital roles in proline-directed phosphorylation-dependent signaling pathways.[3,4] This enzyme acts as a "hub" in the cellular milieu, transiently interacting with and catalyzing multiple targets as they appear and disappear with the tightly regulated activities of proline-directed serine/threonine kinases and phosphatases, respectively.[4,5] Pin1 regulates diverse cellular processes such as cell-cycle progression, cellular stress response, growth-signal response, immune response and neuronal function.[4] Commensurate with its central roles, Pin1 has been implicated in numerous diseases, including cancer, asthma and Alzheimer's disease (AD).[6,7] In contrast to its disease promoting role as an overexpressed protein in human cancers,[8] Pin1 has been shown to play a neuroprotective role in cellular and mouse models of

AD.[9,10] Since the discovery of Pin1[11] and the subsequent demonstration of its functional impacts in cells and organisms,[4] the conformational switch intrinsic to prolyl *cis*−*trans* isomerization has emerged as a new class of molecular timer[12] that plays significant roles in many biological processes.[6,13]

Pin1 belongs to the parvulin class of PPIases and is the prototype for a unique subclass of parvulins that possess a dual-domain architecture composed of separate substrate binding (WW) and catalytic (PPIase) domains.[1,14] The WW domain mediates protein−protein interactions of Pin1 and is essential for its *in vivo* function.[10,15] Members of the WW domain family consist of generally 35 residues, and the family derives its name from two conserved tryptophan residues. On the basis of their specificity to different proline-rich recognition motifs, the WW

domain family is classified into five groups (I–V).[16] Among them only group IV, represented in Pin1, is phosphorylation-dependent and recognizes pS/T-P as its binding motif.[15] Peptide recognition modules, such as WW, SH3, SH2, EH and PTB domains, have been extensively used by nature as functional units to recognize and bind specific short linear sequence motifs (typically two to eight consecutive amino acids).[17,18] Multicellular organisms possess close to 1000 such distinct modules[19] and employ them for protein–protein interactions that form the basis of complex regulatory systems and signaling pathways.[18,20] The presence of the WW domain as a distinct binding module enables Pin1 to interact with various biological substrates and thus participate in numerous signaling pathways.[3,6,21]

Although the structural and thermodynamic details of substrate binding for the Pin1-WW domain have been studied in considerable depth for several ligands, characterization of the binding kinetics has been elusive.[15,22−29] Very rapid dissociation rates preclude quantitative measurement by surface plasmon resonance (SPR), and to date no quantitative binding rates for any Pin1-WW domain/substrate interaction have been reported.[24,30,31] Quantification of the Pin1-WW domain binding kinetics for one of its many cellular targets would provide an important foundation for understanding the transient interaction between this globular binding domain and its short linear peptide recognition motif. For such transient interactions in biological processes, rapid association can be as important as affinity, and slow versus rapid dissociation can provide a critical timer and can facilitate fast responses to changes in cellular targets and conditions.[32,33]

The amyloid precursor protein (APP) is a key biological substrate of Pin1.[10,34] Of particular importance is the observation in both cellular and mouse AD models that Pin1 activity reduces the production of neurotoxic amyloid-β-peptide (Aβ), a major causative agent of AD.[10] The APP intracellular domain (AICD), when phosphorylated at T668 (APP$_{695}$ isoform numbering), adopts distinct *cis* and *trans* isomers of the pT668-P669 peptide bond (Figure 1A) and becomes an important biological substrate of Pin1.[10,35,36] APP undergoes proteolytic processing via two alternative pathways (Figure 1B). The β-secretase-mediated amyloidogenic pathway produces Aβ, while the α-secretase-mediated nonamyloidogenic pathway precludes Aβ formation and generates the neurotrophic APP fragment αAPPs.[37] Phosphorylation of T668 in AICD has been implicated in the amyloidogenic processing of APP,[38] Aβ production[39] and neurodegeneration.[39,40] We have previously shown that Pin1 regulates APP processing, binds *via* its WW domain to the pT668-P669 motif in APP *in vitro* and *in vivo*, catalyzes *via* its PPIase domain the *cis/trans* isomerization of this motif, and inhibits Aβ production.[10] Furthermore, loss of Pin1 function increases APP internalization to compartments where amyloidogenic (Aβ generating) processing occurs, but even with loss of Pin1 function the T668A mutant (which cannot be phosphorylated) is retained at the plasma membrane at normal levels (i.e., comparable to wild type APP in the presence of Pin1 function).[34] Thus, phosphorylation of T668 in APP and the activity of Pin1 are central factors in determining the proteolytic processing fate of APP and thus, the progression of AD.

Previously, we have reported the complete characterization of the thermodynamics and kinetics of the isolated Pin1-PPIase domain interaction with a synthetic peptide that mimics T668-phosphorylated APP (pAPP, Figure 1C).[41] Here we report
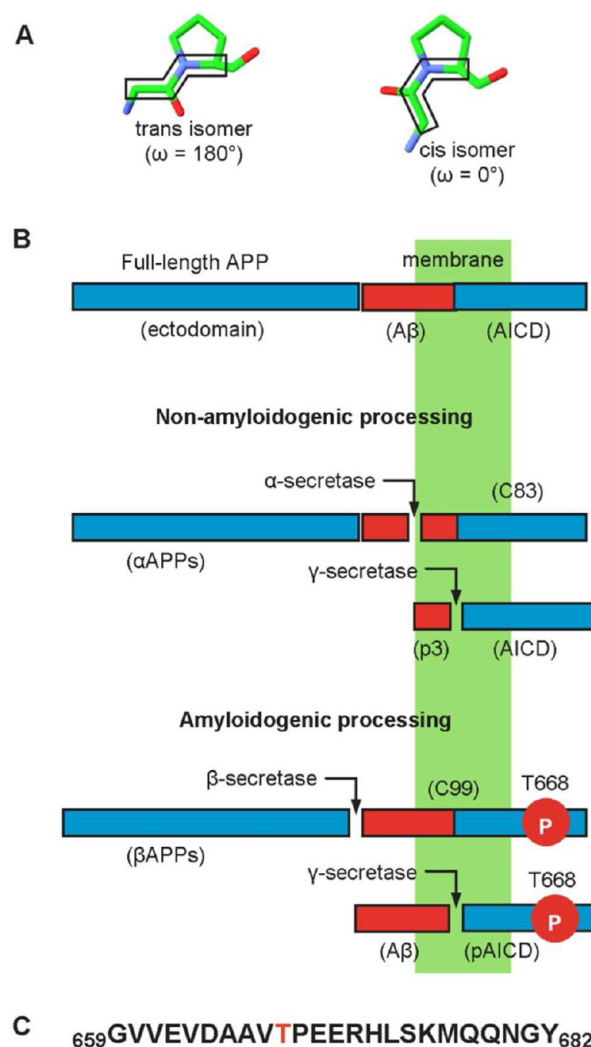

Figure 1. *Trans* and *cis* isomers and APP processing. (A) The *trans* and *cis* backbone conformations for the X-Pro peptide bond (X is any residue). PPIase enzymes catalyze the isomerization of these two conformations. (B) APP is a type I transmembrane protein. In the non-amyloidogenic pathway, it is processed by α- secretase followed by γ-secretase, resulting in the formation of three fragments. The amyloidogenic processing pathway results in the processing of APP by β-secretase then γ-secretase, and the formation of the toxic Aβ-peptide. (C) Sequence of the pAPP-derived peptide, phosphorylated at T668 (red).

nuclear magnetic resonance (NMR), fluorescence, and isothermal titration calorimetry (ITC) studies of the isomer-specific interaction between the isolated Pin1-WW domain and pAPP that provide the kinetic rates for both fast binding (k_{off} = 2040 s^{-1}, k_{on} = 9.9 × 10^7 M^{-1} s^{-1}) and slow isomerization (k_{ct} = 0.0134 s^{-1}, k_{tc} = 0.001 s^{-1}, where k_{ct} is the *cis*-to-*trans* rate and k_{tc} is the *trans*-to-*cis* rate). NMR titration data demonstrate the *trans* isomer specificity of this interaction, in agreement with findings for other Pin1-WW ligands.[16,29] Application of NMR line shape analysis to the titration series of NMR spectra yields the microscopic rate and equilibrium constants for the coupled equilibria of *cis*–*trans* isomerization and *trans*-specific binding, which represents a segment of the overall Pin1 reaction scheme. ITC studies provide an independent measure of the affinity, while time-dependent fluorescence experiments yield the rate of uncatalyzed *cis*–*trans* isomerization of the free ligand. These

results quantify for the first time the binding kinetics of the Pin1-WW domain for a biological Pin1 substrate, and demonstrate that the association rate (near the diffusion limit) and dissociation rate are on the fast end of typical biomolecular interactions.[42−46] The studies presented here also highlight the vastly different time scales of the rapid isomer-specific interaction and slow uncatalyzed *cis*−*trans* isomerization, and quantify key steps in the Pin1 reaction scheme for this substrate. Furthermore, these studies highlight the powerful combination of NMR line shape analysis, fluorescence, and ITC for obtaining a complete thermodynamic and kinetic description of isomer-specific interactions, especially those with fast binding kinetics.

■ MATERIALS AND METHODS

Peptide and WW Domain Preparation. Purified ^{15}N-labeled and unlabeled phosphopeptides representing APP residues 659−679 (pAPP659−679) and 659−682 (pAPP659−682, Figure 1C) phosphorylated at T668 were purchased from the Tufts University Core Facility, Boston, MA. To provide site-specific probes for NMR, ^{15}N was selectively incorporated at the amide nitrogen of residues V667 and E670 ([15]N-[V667,E670]-pAPP659−679). Phosphopeptide concentrations were determined by dry weight (for pAPP659−679) before dissolving in desired buffer, or by UV absorbance at 280 nm (for pAPP659−682, using $\varepsilon_{280} = 1280$ cm^{-1} M^{-1} for a solvent-exposed tyrosine residue) of the phosphopeptide solution. Two WW domain constructs, WW50 (Pin1 residues 1−50) and WW53 (Pin1 residues 1−53), were employed. The WW domain was encoded in the pET28 a(+) vector and expressed as a N-terminal His$_6$-tagged fusion protein, with a thrombin cleavage site, in Kanamycin resistant BL21-DE3 *Escherichia coli* cells. To obtain ^{15}N-labeled WW domain, bacteria were grown in M9 minimal media at 37 °C with [15]NH$_4$Cl as the sole nitrogen source. For unlabeled WW domain, bacteria were grown in LB media. Protein expression was induced with 1 mM isopropyl β-D-1-thiogalactopyranoside when the OD$_{600}$ reached 0.8, and cells were harvested after 4 h. Cells were lysed in 20 mL of wash buffer (25 mM HEPES, 300 mM or 150 mM NaCl, 10 mM Imidazole, pH = 7.5) with 100 μL of protease inhibitor (PI) cocktail and 5 mg of lysozyme added, and sonicated on ice. Cell debris was removed by centrifugation and the supernatant was passed through 2 mL of Ni-column pre-equilibrated with wash buffer. The column was washed with 10 bed volumes of wash buffer and 5 bed volumes of cleavage buffer (20 mM Tris-HCl, 150 mM NaCl, 2.5 mM CaCl$_2$, pH = 8.4) leaving 1 bed volume of the cleavage buffer in the column. Biotinylated thrombin (Novagen Thrombin Cleavage Capture kit) was used to cleave the WW domain on the column. The cut protein product contained additional residues (G-S for WW50 and G-S-H for WW53) from the thrombin cut-site and cloning at the N-terminus. WW domain concentration in samples used for experiments was measured by UV absorption at 280 nm ($\lambda_{280} = 13980$ cm^{-1} M^{-1}). The thrombin was removed by adding streptavidin-agarose beads that were separated from cut WW domain by spin columns. WW domain purity was verified by SDS-PAGE. The purified protein was dialyzed into HEPES buffer (10 mM HEPES, 10 mM NaCl, 1 mM DTT, 5 mM NaN$_3$, pH = 6.9) overnight at 4 °C. For NMR experiments, 5 μL of PI cocktail was added to 300 μL of protein sample.

Isothermal Titration Calorimetry (ITC). Isothermal titration calorimetry experiments were performed at 25 °C

using a Calorimetry Sciences Corporation (Lindon, UT) Nano-ITC Series III instrument. Purified WW53 was dialyzed into HEPES buffer overnight at 4 °C. The pAPP659-682 was first dissolved in deionized water and pH-adjusted to 6.9, was then lyophilized, and the lyophilized powder was dissolved in the same buffer to yield a final concentration of 3.1 mM (determined by A_{280}). WW53 and peptide solutions were degassed for 10 min prior to each experiment. The reaction cell was filled with 1.2 mL of 177 μM WW53. The 250 μL syringe was filled with 3.1 mM pAPP659-682, and was titrated in 31 injections of 8 μL each. The cell volume was 1024 μL. Injections were made at 8 min intervals to allow the signal to decay to baseline. The reaction mixture was stirred at 200 rpm. To determine the heat of dilution of pAPP659-682, the reaction cell was filled with HEPES buffer, and 8 μL of 3.1 mM pAPP659-682 was injected at 5 min intervals for a total of 20 injections. The commercial software BindWorks 3.1 (Calorimetry Sciences Corporation) was used to determine peak volumes, to subtract the heat of dilution, and to construct the corresponding binding isotherm.

The binding isotherm was fit by nonlinear regression to eq A1, expressed in terms of eqs A2 and A5, as described in detail in the Appendix. Random noise, scaled by the residuals of the best fit, was added to the data to generate 1000 synthetic data sets that were fit to eq A1 in the same manner. Reported errors in the fitting parameters are the standard deviations of these fitted parameters. All fitting of real and synthetic ITC data was done with in-house codes written in MATLAB 2010a.

NMR Titration Experiments. Four titration experiments were performed: ^{15}N-labeled peptide ([15]N-[V667,E670]-pAPP659-679) titrated with unlabeled WW53, ^{15}N-labeled WW50 titrated with unlabeled peptide (pAPP659-682, containing a native C-terminal tyrosine that allows accurate UV quantification of its concentration, Figure 1C), ^{15}N-labeled WW50 titrated with sodium phosphate (NaH$_2$PO$_4$), and ^{15}N-labeled WW50 titrated with HEPES. Because the binding motif is located about 10 residues from the C-termini of these two peptides, for the purposes of measuring WW domain binding these two peptides are indistinguishable. For the ^{15}N-peptide titration, the most saturated sample was prepared first, containing 0.65 mM peptide and 1 mM WW53. In the subsequent titration steps, part of the previous sample was diluted with 0.65 mM peptide to obtain the required molar ratio and a final volume of 300 μL. Eight titration points were collected; the ^{15}N peptide concentration was kept constant at 0.65 mM while the WW53 concentration was 0, 0.01, 0.05, 0.10, 0.20, 0.33, 0.50, or 1.0 mM. Similarly, for the ^{15}N-WW50 peptide titration, the most saturated sample was prepared first, containing 0.35 mM ^{15}N-WW50 and 3.9 mM peptide. The subsequent steps were obtained by diluting with a stock solution of 0.35 mM ^{15}N WW50. Twelve titration points were collected with peptide concentrations of 0, 0.04, 0.06, 0.09, 0.13, 0.19, 0.29, 0.43, 0.65, 0.98, 1.95, and 3.90 mM. For the ^{15}N-WW50 phosphate titration, the apo ^{15}N-WW50 sample (concentration of 0.43 mM) was prepared first, and subsequent samples were prepared by adding small volumes of stock solutions of either 100 mM or 1 M sodium phosphate. Nine titration points were taken with phosphate concentrations of 0, 0.8, 4.2, 8.3, 16.8, 30.7, 48.9, 102, and 197 mM. In the same manner, for the ^{15}N-WW50 HEPES titration, six titration points were obtained with HEPES concentrations of 0, 10, 20, 100, 200, and 400 mM. For each titration point a [15]N−^{1}H HSQC spectrum was collected. All experiments were carried

out at 25 °C on a Varian Inova 600-MHz spectrometer. For the ^{15}N-labeled WW50 titrations, 2048 × 256 complex data points and for the ^{15}N-labeled peptide titrations, 2048 × 128 complex data points were acquired. The exponential decay window function was applied to peptide titration data in order to preserve the Lorentzian line shape, and a 90° phase-shifted sine bell window function was applied to the phosphate and HEPES titration data. Following apodization, all data sets were zerofilled and Fourier transformed using NMRPipe (http://spin.niddk.nih.gov/NMRPipe/).

Dissociation Constants from Chemical Shift Titrations. The dissociation constant (K_D) for *trans* ^{15}N-[V667,E670]-pAPP659-679 binding to WW53 was determined by fitting the chemical shift changes in the NMR titration experiment. For this titration, single-dimension chemical shift changes were employed ($\Delta\delta_H = \delta_H^{obs} - \delta_H^{free}$ for the proton dimension, and $\Delta\delta_N = 0.154 \times (\delta_N^{obs} - \delta_N^{free})$ for the ^{15}N-dimension, where δ_i^{free} and δ_i^{obs} are the apo and titration point-specific observed chemical shifts, respectively, for nucleus i = H or N). Three independent data sets ($\Delta\delta_H$ versus WW53 concentration for V667 and E670, and $\Delta\delta_N$ versus WW53 concentration for E670) were fit simultaneously. As shown in Results, this binding interaction is *trans*-specific and involves coupling between the *cis*−*trans* isomerization and binding equilibria (*vide infra*). The change in chemical shift at each titration point, accounting for the coupled equilibria, is given by

$$\Delta\delta_i = \frac{[\text{WW:T}] \times (\delta_i^{bound} - \delta_i^{free})}{[\text{WW:T}] + \{[L^{tot}] - [\text{WW:T}]\}[K_{isom}/(1 + K_{isom})]} \quad (1)$$

where i = H or N, $[L^{tot}]$ is the total ligand concentration, δ_i^{bound} is the chemical shift of the bound species of nucleus i, K_{isom} is the equilibrium constant of *cis*−*trans* isomerization, and $[\text{WW:T}]$ is the bound *trans* concentration, determined from

$$[\text{WW:T}] = \frac{1}{2}(K_D^{app} + [\text{WW}^{tot}] + [L^{tot}]$$
$$- \sqrt{(K_D^{app} + [\text{WW}^{tot}] + [L^{tot}])^2 - 4[\text{WW}^{tot}][L^{tot}]}) \quad (2)$$

where $[\text{WW}^{tot}]$ is the total concentration of WW domain, and K_D^{app} is the apparent dissociation constant given by

$$K_D^{app} = K_D\left(1 + \frac{1}{K_{isom}}\right) \quad (3)$$

where K_D is the dissociation constant of *trans* peptide binding to the WW domain. K_D and δ_i^{bound} were obtained by fitting the measured $\Delta\delta_i$ versus $[\text{WW}^{tot}]$ to eqs 1−3 using nonlinear regression. Since pAPP659−679 has no aromatic residues (i.e., no near UV absorbance), an additional fitting parameter, L^{corr}, was used to correct the weight-based total ligand concentration, $[L^{measured}]$,

$$[L^{tot}] = [L^{measured}] \times L^{corr} \quad (4)$$

Errors in the fitting parameters were determined by adding normally distributed random noise scaled by the residuals of the best fit to the experimental data and performing 1000 Monte Carlo simulations.

The dissociation constants for phosphate and HEPES binding to WW50 were determined from the composite chemical shift change, given by

$$\Delta\delta = \sqrt{(\delta_H^{obs} - \delta_H^{free})^2 + (0.154 \times (\delta_N^{obs} - \delta_N^{free}))^2} \quad (5)$$

Observed chemical shift changes were fitted to the corresponding binding equation to determine K_D and δ^{bound},

$$\Delta\delta = \frac{[\text{WW}^{bound}] \times (\delta^{bound} - \delta^{free})}{[\text{WW}^{tot}]} \quad (6)$$

where δ^k is the composite chemical shift of state k (k = bound or free, $\delta^k = ((\delta_H^k)^2 + (0.154 \times \delta_N^k)^2))^{1/2}$, the bound WW domain concentration $[\text{WW}^{bound}]$ is given by eq 2, but with $[\text{WW:T}]$ replaced with $[\text{WW}^{bound}]$ and K_D^{app} replaced with the true dissociation constant, K_D. Errors in the fitting parameters were obtained by taking the standard deviations of these parameters from individual fits of binding curves for five residues in the case of phosphate titration, and three residues for the HEPES titration.

NMR Lineshape Analysis. Lineshape analysis of the ^{15}N-WW50 titration with pAPP659−682 was performed using the *BiophysicsLab* Matlab package (currently, Integrative Data Analysis Platform, IDAP;[47] http://kovrigin.chem.mu.edu/IDAP/) as previously described.[41] For a given peak in a ^{15}N−^{1}H HSQC spectrum from the titration series, the 1D slices through the center of the peak in each dimension (^{1}H, ^{15}N) were treated as independent data sets. The area under the line shape of each slice was normalized to eliminate the decrease in signal intensity due to any line broadening occurring in the orthogonal dimension. This normalization process also effectively eliminates any titration-dependent variations in coherence losses during INEPT transfer delays in the ^{15}N−^{1}H HSQC pulse sequence.

For the line shape fitting, the equilibrium populations of the free WW domain, $p_{free} = ([\text{WW}^{free}]/[\text{WW}^{tot}])$ and *trans*-bound WW domain, $p_{bound} = ([\text{WW:T}]/[\text{WW}^{tot}])$, were determined from a three-state model that includes the coupled equilibria of *cis*−*trans* isomerization and *trans*-specific binding (*vide infra*), using eq 2 and the relationship

$$[\text{WW}^{free}] = [\text{WW}^{tot}] - [\text{WW:T}] \quad (7)$$

To correct for small errors in protein and peptide concentration measurements, the correction factor L^{corr} is applied to the measured peptide concentration as described by eq 4.

BiophysicsLab was used to fit the 1D slices from the titration data to the two-state solution to the Bloch-McConnell equations.[48,49] The population (p_{free} or p_{bound}) of each species was calculated using the thermodynamic equations above, for the known total protein and total peptide concentrations for each titration point. Fitted parameters included the dissociation rate (k_{off}), dissociation constant (K_D), concentration correction factor (L^{corr}), and substrate-bound chemical shift (δ^{bound}). Constrained parameters included linewidths of both free and bound states ($R_{2,0}^{free}$ and $R_{2,0}^{bound}$, respectively), and the free chemical shift (δ^{free}).

The rate constants (k_i) are expressed in a rate-matrix that is derived from the equilibrium rate equations for each species. The calculated line shape is given by eq 8,

$$S(\nu) = \text{SF} \cdot \text{Re}\left([1\ 1](M_1 + M_2)^{-1}\begin{bmatrix} p_{free} \\ p_{bound} \end{bmatrix}\right) \quad (8)$$

where

$$M_1 = \begin{pmatrix} R_{2,0}^{\text{free}} & 0 \\ 0 & R_{2,0}^{\text{bound}} \end{pmatrix} - \begin{pmatrix} k_{\text{on}}[L^{\text{free}}] & -k_{\text{off}} \\ -k_{\text{on}}[L^{\text{free}}] & k_{\text{off}} \end{pmatrix}$$
$$- 2\pi i \begin{pmatrix} \nu^{\text{free}} & 0 \\ 0 & \nu^{\text{bound}} \end{pmatrix} \tag{9}$$

$$M_2 = 2\pi i \nu \begin{pmatrix} 1 & 0 \\ 0 & 1 \end{pmatrix} \tag{10}$$

In the above equations, parameters are as defined above, ν is the chemical shift variable (in Hz), ν^{free} and ν^{bound} are the chemical shifts of the free and bound states (in Hz), respectively, $[L^{\text{free}}]$ is the concentration of free peptide ($[L^{\text{free}}] = [L^{\text{tot}}] - [\text{WW:T}]$), and SF is a scaling factor that is fitted individually for each residue. The matrix M2 represents the chemical shift variable ν in matrix form. The sum of squares of the residuals (SS) was used to determine the quality of fit. It is determined as

$$SS = \sum_{j}^{M} \sum_{i}^{N_j} \frac{(f_{ij} - y_{ij})^2}{\sigma_j^2} \tag{11}$$

where f_{ij} and y_{ij} are the fitted and actual NMR signal at a frequency point i respectively, σ_j is the spectral noise given by the rmsd of the baseline of spectrum 'j', N_j is the number of data points in spectrum 'j' and M is the number of titration points. In the iterative fitting process, the fitted parameters were varied to minimize SS. Errors in the fitting parameters were estimated using Monte Carlo simulation. The random variation of experimental data for Monte Carlo fitting trials was obtained by applying Gaussian noise to experimental spectral intensities according to the RMSD of the spectral noise floor.

Measurement of Intrinsic Isomerization Rate by Fluorescence Spectroscopy. For a given isomer-specific protein/peptide interaction in which the fluorescence signal changes with binding of the selected peptide isomer (e.g., the *trans* isomer), it is possible to measure the intrinsic rate of peptide isomerization. When the protein is mixed with a substoichiometric amount of peptide, binding occurs over two disparate time scales: a fast phase in which the protein binds the initial *trans* isomer of the peptide, and a slow phase in which the initial *cis* isomer of the peptide converts to *trans* and subsequently binds. Equilibrium is reached during this slow phase according to an exponential function,

$$I(t) = I_{\text{final}} + (I_0 - I_{\text{final}})e^{-tk_{\text{obs}}} \tag{12a}$$

where $I(t)$ is the time-dependent fluorescence intensity, I_0 and I_{final} are the fluorescence intensity at the first measured point and after equilibrium has been reached, respectively. The rate constant k_{obs} is given by (derived in the Appendix),

$$k_{\text{obs}} = k_{\text{ct}} + k_{\text{tc}}/(1 + [\text{WW}^{\text{free}}]/K_D^{\text{app}}) \tag{12b}$$

where k_{ct} and k_{tc} are the *cis*-to-*trans* and *trans*-to-*cis* isomerization rates, $[\text{WW}^{\text{free}}]$ is the concentration of free WW domain, and K_D^{app} is defined by eq 3. Because the tryptophan fluorescence signal of the WW domain increases slightly upon binding the pAPP659−682 peptide, it is possible to measure the kinetics of this slow phase by monitoring the fluorescence signal of the mixture as a function of time.

Tryptophan fluorescence experiments were performed using a F-7000 fluorescence spectrophotometer (Hitachi High

Technologies America, Schaumburg, IL). Protein solution (0.42 mM, 2 mL) was equilibrated in a gently stirred quartz cuvette that was temperature controlled at 25 °C. Fifteen microliters of a 20 mM stock of pAPP659-682 peptide was then added to the cuvette, for a final peptide concentration of 0.15 mM, and a 10 min time course was recorded in 0.2 s intervals. Fluorescence intensity was measured by exciting at 298 nm and detecting at 337 nm (2.5 nm bandpass for excitation slit, 20 nm bandpass for emission slit). Before fitting, fluorescence data was subjected to subtraction of a baseline, which was measured by taking data of WW domain before addition of peptide. The k_{ct} and k_{tc} values were determined from the measured k_{obs} using eq 12b with the calculated equilibrium value of free WW domain, 0.28 mM, and the NMR-determined K_{isom} value of $K_{\text{isom}} = k_{\text{ct}}/k_{\text{tc}} = 13.6$. Data fitting was performed using the entire data set, but for display purposes fluorescence data were averaged over 5 s intervals.

■ RESULTS

Quantification of Buffer Interactions with the Pin1-WW Domain. A direct interaction of the Pin1-WW domain (hereafter referred to as WW domain) binding surface with buffer anions has potential implications for quantification of the binding function of this domain in anionic buffers such as phosphate. Many previously reported studies of this WW domain have utilized phosphate buffer, and most of the functional and quantitative measurements on this domain have been performed in the presence of phosphate ions.[26,50,51]

To quantify the binding of the WW domain to phosphate ions, sodium phosphate was titrated into ^{15}N-WW50 in HEPES buffer at pH 6.9, 298 K. The affinity was quantified by shifts in peaks arising from residues M15, S16, G20, V22 and Y23 (Figure 2A), yielding a dissociation constant (K_D) of 56 ± 6 mM (Figure 2B). These residues, which displayed the largest chemical shift changes when phosphate was added, are in or near the phosphate binding pocket (defined as the side chains of S16 and R17 and the backbone amide of R17 [16]). The R17 and S18 peaks also display large chemical shift changes with addition of phosphate. Although broadened beyond the limit of detection in the absence of phosphate, the R17 and S18 peaks emerged at higher phosphate concentrations (Figure 2B) and at lower pH (Supplemental Figure S1, Supporting Information), consistent with amide exchange broadening. Since the R17 and S18 peak positions are invariant above pH 5.6 in HEPES buffer (Supplemental Figure S1, Supporting Information), these static peak positions were used for the free ^{15}N and ^{1}H chemical shifts of each residue at pH 6.9. The bound ^{15}N and ^{1}H chemical shifts for R17 and S18 were determined from fitting of the few observed peaks for each residue in the phosphate titration series, constraining the K_D value to the already determined value of 56 mM. The resulting chemical shift difference between free and bound states for R17 (S18) is 2.87 ppm (0.79 ppm) in the ^{15}N-dimension, and 0.83 ppm (0.37 ppm) in the ^{1}H dimension, suggesting close proximity of these NH groups to bound anion.

These results, in particular the large chemical shift changes of the R17 and S18 backbone amide groups (Figure 2B), indicate coordination of the phosphate group in the phosphate binding pocket and is consistent with the structure of WW domain bound to RNA polII C-terminal domain peptide.[16] Importantly, the binding constant of ∼56 mM demonstrates that at 10 mM buffer phosphate and 1 mM WW domain concentration, 15% of WW domain will be bound to phosphate. HEPES is also an
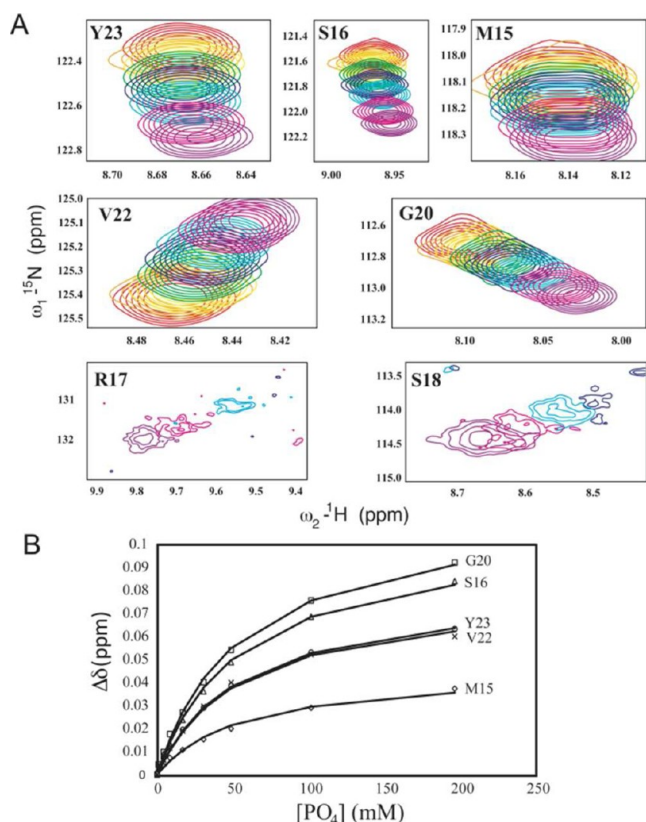
Figure 2. Interaction of Pin1-WW domain and phosphate. (A) Overlays of $^{15}N-^{1}H$ HSQC spectra of ^{15}N labeled Pin1-WW domain titrated with phosphate (Na_2HPO_4). Concentrations were 0 (red), 0.8, 4.2, 8.3, 16.8, 30.7, 48.9, 101.7, and 196.6 (purple) mM phosphate and 0.43 mM WW domain. Residues R17 and S18 were broadened beyond the limits of detection in the apo spectrum due to amide exchange with the solvent, but emerged as saturation with phosphate was approached. (B) Composite chemical shift changes, defined as $\Delta\delta = ((\delta_H - \delta_H^{free})^2 + (0.154 \times (\delta_N - \delta_N^{free}))^2)^{1/2}$, as a function of phosphate concentration. The chemical shifts δ^{free} are obtained from the apo spectrum. The data were fit to yield a dissociation constant (K_D) of 56 ± 6 mM (average ± standard deviation). Data points are shown as open symbols and fits are shown as lines.

anionic buffer that is widely used for Pin1 functional studies.[52−54] The interaction of HEPES with WW50 is weaker (149 ± 36 mM, determined from composite chemical shift changes of Q33, W34 and E35 in response to HEPES addition, Supplemental Figure S2, Supporting Information), corresponding to 6% HEPES-bound WW domain under the same conditions (10 mM HEPES, 1 mM WW domain). Therefore, to maintain consistency with widely employed Pin1 buffer conditions and to minimize populations of buffer-bound WW domain, HEPES buffer was used for all of the NMR and ITC studies reported below.

Isomer-Specific Interaction of Phospho-T668 APP with the WW Domain. Previously, we reported that addition of an equimolar amount of isolated WW domain to an APP phosphopeptide (APP residues 659−679 phosphorylated at T668 and ^{15}N-labeled at E670) caused peak shifts for both the *cis* and *trans* isomers, suggesting similar affinity for these distinctly different structures.[10] In order to more fully characterize the isomer specificity of this interaction, ^{15}N-labels were incorporated at both V667 and E670, the chemical environments of which are sensitive to the isomeric states of
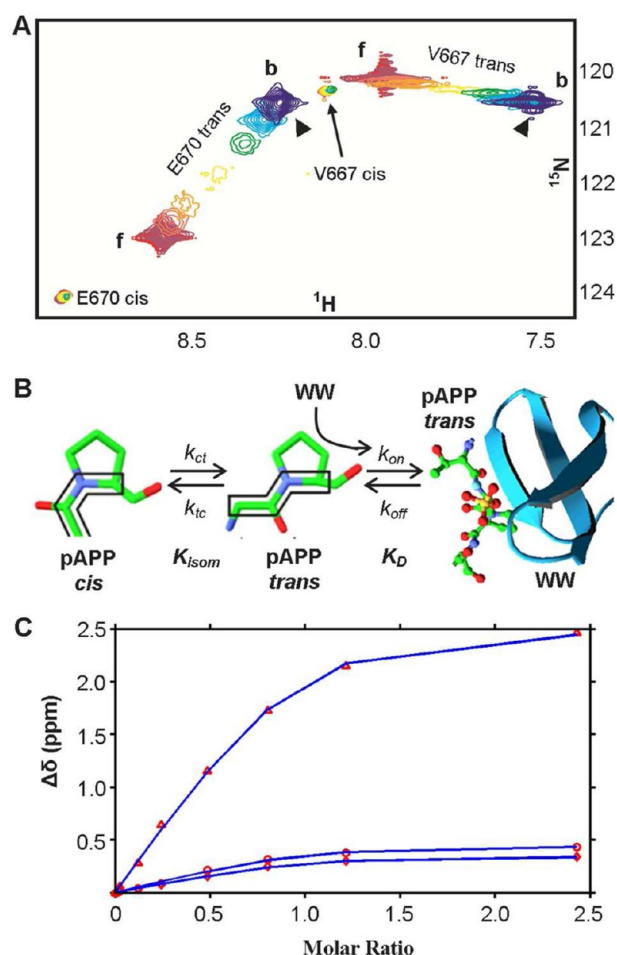

Figure 3. Interaction of Pin1-WW domain and pAPP-derived phosphopeptide, from the ^{15}N-labeled phosphopeptide perspective. (A) Overlays of $^{15}N-^{1}H$ HSQC spectra of ^{15}N-[V667,E670]-pAPP659−679 titrated with unlabeled WW53; 'f' denotes free and 'b' bound peptide. Concentrations were phosphopeptide = 0.65 mM; WW53 = 0.01, 0.05, 0.1, 0.2, 0.33, 0.5, or 1 mM. Peaks in the spectrum with highest WW53 concentration are denoted by arrowheads; peaks for the *cis* isomer in this spectrum are not observed. (B) Interaction scheme of WW domain with pAPP, including isomerization of free *cis* and *trans* and *trans*-isomer binding to the WW domain. (C) Quantification of the dissociation constant, K_D, from ^{1}H chemical shift changes of V667 (O) and E670 (◇), and ^{15}N chemical shift changes of E670 (Δ).

the pT668-P669 peptide bond, and a multistep titration with unlabeled WW domain was performed (Figure 3A).

Titration experiments in HEPES buffer were performed by keeping the concentration of ^{15}N-[V667,E670]-pAPP659-679 peptide constant, and recording $^{15}N-^{1}H$ HSQC spectra with different concentrations of WW53. During the titration, the peaks corresponding to the *trans* isomer move from free to bound positions and exhibit ligand-induced exchange broadening (Figure 3A), indicating that binding is in fast exchange relative to the NMR time scale. Notably, at and near equimolar concentrations, the *trans* peak is considerably broadened. The corresponding peaks of the *cis* isomer do not significantly move, and gradually diminish via conversion to the *trans* isomer as the concentrations of free *cis*, free *trans* and bound *trans* equilibrate with addition of WW53 (Figure 3A). In the previously reported work,[10] the single titration point was near-equimolar, where the *trans* peak intensity would be significantly diminished due to
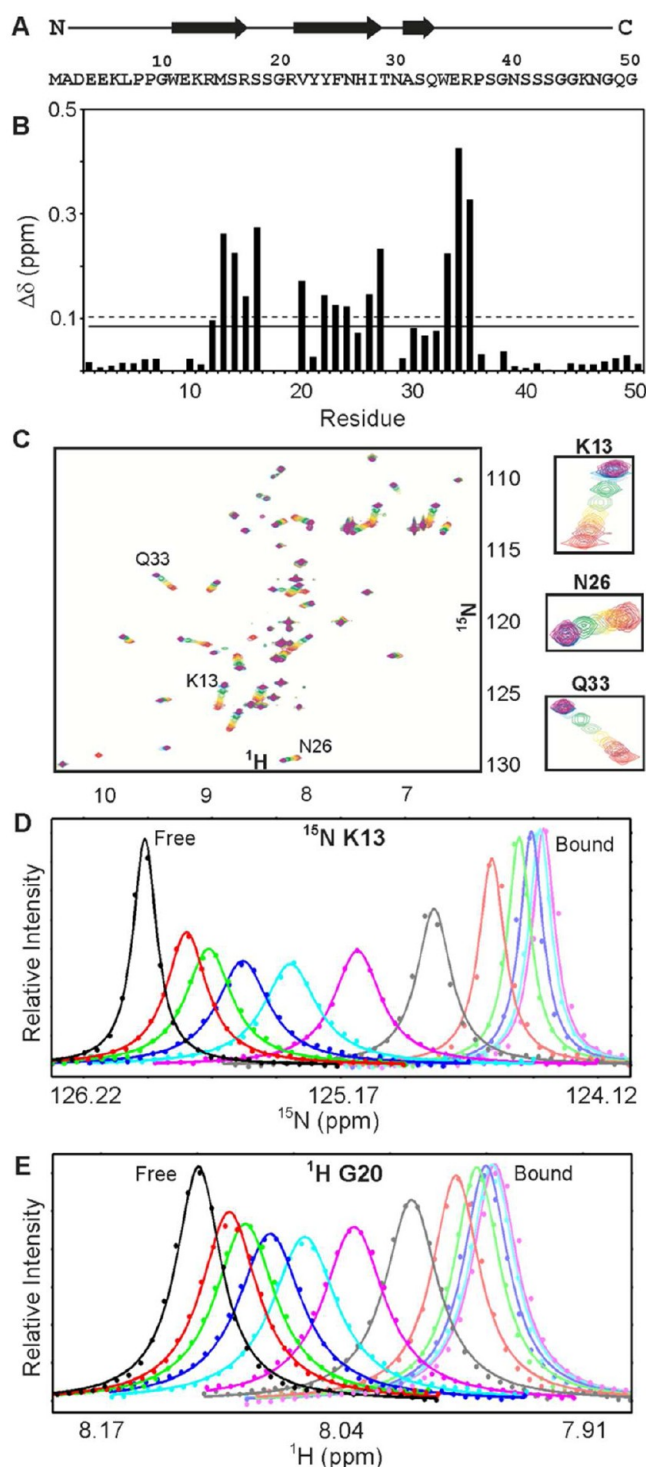
Figure 4. Interaction of Pin1-WW domain and pAPP derived phosphopeptide, from the ^{15}N-labeled WW domain perspective (A) Primary sequence and the secondary structure elements of the Pin1-WW domain. (B) Composite chemical shift change, $\Delta\delta = ((\delta_H^{bound} - \delta_H^{free})^2 + (0.154 \times (\delta_N^{bound} - \delta_N^{free}))^2)^{1/2}$, for each ^{15}N-WW50 residue between the free and pAPP659−682-bound states. The chemical shifts δ^{free} and δ^{bound} are obtained from the apo and the most saturated spectra of ^{15}N WW50, respectively. The solid and broken lines represent the mean and the significance level (mean + standard deviation) of the chemical shift perturbation. (C) ^{15}N−^{1}H HSQC of ^{15}N WW50 titration with unlabeled pAPP659−682, red (free), through purple (bound). Insets show expanded views of example peak trajectories through the course of titration. (D, E) NMR line

shape simulation results. The 1D slices of NMR data (●) and simulated lineshapes (—) for two representative ^{15}N−^{1}H HSQC WW50 peaks resulting from simultaneous fitting of the seven selected data sets (see main text). (D) The ^{15}N dimension of the ^{15}N−^{1}H HSQC peak for residue K13. (E) The ^{1}H dimension of the ^{15}N−^{1}H HSQC peak for residue G20.

exchange broadening. Furthermore, the chemical shifts of the E670 amide group are highly sensitive to pH in the range of 5−7 due to its interaction with the titrating phosphate group[36] (Supplemental Figure S3, Supporting Information). The chemical shift change of the single ^{15}N-labeled E670 *cis* peak observed in the earlier work[10] is attributed to a pH change of the sample upon WW domain addition. The current results clarify that the *cis* interaction with the WW domain is very weak (based on sensitivity considerations, $K_d^{cis} \geq 13$ mM). Thus, consistent with findings for other Pin1-WW domain ligands,[16,29] the interaction with the pS/T-P motif in APP is *trans*-specific. Moreover, because the *cis* isomer binding is negligible, the simplest binding scheme involves two equilibration steps: *cis*−*trans* isomerization and *trans*-specific binding (Figure 3B). Using this model, fitting of the ^{1}H (for V670 and E668) and ^{15}N (for V670) chemical shift changes induced by titration of WW53 yielded $K_D = 26.9 \pm 8.8$ μM (Figure 3C).

Determination of Binding Affinity and Kinetic Parameters by NMR Line Shape Analysis. In order to detect the isomer-specific binding process with multiple probes simultaneously, ^{15}N-labeled WW50 was titrated with unlabeled phosphopeptide (pAPP659-682) and monitored by ^{15}N−^{1}H HSQC NMR spectroscopy. The effect of the *trans* isomer binding is sensed throughout the core of the domain, in agreement with previous studies of WW domain binding to other ligands.[29,55] Strikingly, out of 26 residues (G10 to E35) that constitute the β-meander structure of the WW domain (Figure 4A), 18 backbone amides show large chemical shift change in response to pAPP659-682 binding (Figure 4B). Similar to the ligand perspective, ^{15}N-WW50 peaks move and progressively broaden with addition of ligand, and then become narrow as saturation is reached (Figure 4C). These numerous backbone NH groups provide multiple sensors throughout the protein with which to measure the kinetic and thermodynamic parameters for this interaction.

The ^{15}N-WW50 titration data was subjected to line shape analysis as implemented in BiophysicsLab (currently—IDAP; http://kovrigin.chem.mu.edu/IDAP/)[41,47] using the 3-state reaction scheme (Figure 3B). Since the uncatalyzed *cis*−*trans* exchange rate is very slow (time constant on the order of minutes), this rate does not affect the NMR lineshapes and only affects the populations of the two isomers. Hence, the NMR lineshapes were fit to a two state model (free and bound WW domain) while accounting for the thermodynamic coupling to the *cis*−*trans* isomerization equilibrium (Figure 3B). The equilibrium constant for the free *cis*−*trans* isomerization step (K_{isom}) was determined from peak volumes corresponding to the *trans* (V_T) and the *cis* (V_C) isomers in the ^{15}N−^{1}H HSQC spectrum of the free peptide (Figure 3A), and was treated as a constant ($K_{isom} = (V_T/V_C) = 13.6$) in the fitting. The fitting parameters were the dissociation constant (K_D), the off rate (k_{off}) and the chemical shift of the bound species (δ^{bound}), since complete saturation was not reached in these titration experiments. The parameters K_D and k_{off} were

treated as global parameters (same for all titration-sensing residues) and δ^{bound} as a local parameter (unique to each nucleus). The two dimensions, ^{15}N and ^{1}H, for each peak were treated as separate data sets.

All 18 residues in the ^{15}N WW domain that display appreciable chemical shift changes in at least one of the two spectral dimensions upon peptide binding gave rise to peaks that were resolved through the entire course of the titration (Figure 4C). A total of 23 data sets (both dimensions for five peaks, a single dimension for the remaining 13 peaks) were subjected to line shape analysis (Figure 4D,E and Supplemental Table S1, Supporting Information). From these, seven data sets (K13-^{15}N, S16-^{1}H, G20-^{1}H, H27-^{1}H, Q33-^{1}H, W34-^{1}H and E35-^{1}H) for residues that displayed the largest chemical shift changes with titration (and hence, yielded the highest resolution in terms of chemical shift sensitivity to the binding event) were selected for simultaneous fitting. The simultaneous fitting yielded $K_D = 22.4 \pm 0.4$ μM (best fit $\pm95\%$ confidence interval), $k_{off} = 2040 \pm 31$ s^{-1} (with corresponding $k_{on} = (9.1 \pm 0.21) \times 10^7$ M^{-1} s^{-1}) and $L^{corr} = 1.156 \pm 0.002$, where the confidence intervals were computed from Monte Carlo simulations and propagation of errors. This analysis, using the simplest binding scheme for this system (which accounts for both *cis−trans* isomerization and *trans*-specific binding), yielded excellent line shape fits (Figure 4D,E, Supplemental Figure S4 and Supplemental Table S1). In order to test whether these fitted global parameters (k_{off}, k_{on}, K_D) truly represent a global event, they were held constant in the line shape analysis for the 16 additional data sets, fitting only for the chemical shift of the bound species (δ^{bound}). The quality of fit, measured by the sum-of-squares of the residuals (SS), was very similar for the global and individual fitting of the 23 data sets (Supplemental Table S1, Supporting Information). Thus, the parameters obtained from the simultaneous fitting truly represent the global behavior of the binding interaction.

Determination of Binding Affinity by ITC. ITC was used to independently determine the dissociation constant for the interaction between the peptide (pAPP659-682) and the WW domain in HEPES buffer (pH 6.9) at 298 K. Since the binding reaction scheme (Figure 3B) involves both isomerization and binding, the coupled equilibrium must be considered in order to properly determine K_D, as described in the Appendix. Upon injection of the peptide into the reaction cell containing WW53, exothermic peaks were observed which displayed a slow decay to the baseline (Figure 5A). This reflects the two physical processes in the coupled equilibrium reaction scheme (Figure 3B), i.e., fast binding and slow isomerization. The free *trans* isomer in the injected volume binds rapidly to the WW domain and results in the depletion of free *trans*. Equilibrium of the system in the reaction cell is eventually reached through slow isomerization of the free *cis* and *trans* isomers and subsequent binding of newly generated *trans* isomer. The binding isotherm (Figure 5B) was fit to eq A1 (Appendix), derived for the NMR-determined model that accounts for both fast binding and slow isomerization. This fitting, which used the NMR-determined K_{isom} value of 13.6, yielded $K_D = 27 \pm 2$ μM, where the error is the standard deviation obtained from Monte Carlo simulations. In excellent agreement with this ITC-determined K_D, fitting of the NMR chemical shift perturbations for the ^{15}N-[V667,E670]-pAPP659-679 peptide titrated with WW53 yielded $K_D = 26.9 \pm 8.8$ μM (Figure 3C). As illustrated in this analysis, the ITC and NMR approaches are highly complementary in the case of isomer-specific binding, since
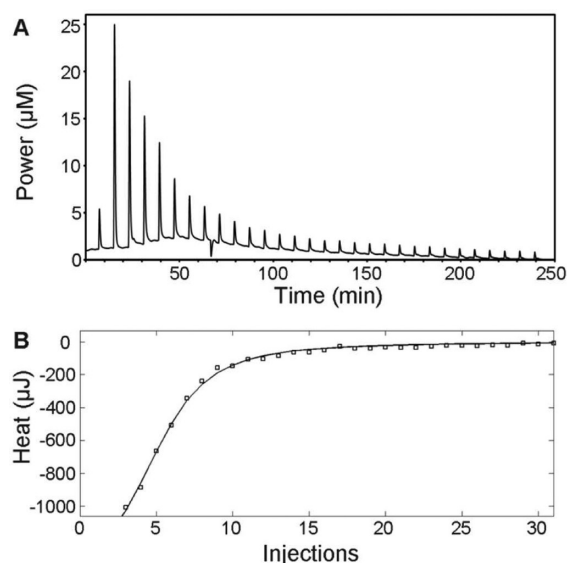

Figure 5. Measurement of K_D for the WW53 interaction with pAPP659−682 by ITC. (A) The raw ITC data and (B) fitting of the binding isotherm data to eq A1. Open squares (□) represent heat evolved per injection and solid line (—) is the fitting to eq A1.

NMR was needed for determination of the correct model (Figure 3B) and for measurement of K_{isom}.

It should be noted that the binding isotherm is not sensitive to the relative contributions of binding and isomerization to the total enthalpy (ΔH_b and ΔH_{ct}, respectively), and so the distinction between ΔH_b and ΔH_{ct} (see Appendix) is tenuous. While the total heat evolved during a given injection is well-determined, the relative contributions from binding and isomerization to this total heat is not. This is because the fraction of total heat due to binding and to isomerization remains nearly constant for each injection, yielding insensitivity of the shape of the isotherm curve to this ratio. Simulations of ITC data with the ratio of ΔH_b to ΔH_{ct} varying between 10 and 0.1 yielded isotherm curves for which the standard deviation of their difference was only 0.1%. In principle, the large temporal separation between binding and *cis−trans* isomerization would allow ΔH_b and ΔH_{ct}, along with the kinetics of *cis−trans* isomerization to be determined from fitting of the shape of individual isotherm peaks using the theoretical framework provided in the Appendix. However, this requires a modern ITC apparatus with well-determined response time and mixing time.[56] The older generation ITC instrument employed for these studies unfortunately precluded this level of analysis of the acquired data.

Weak WW-Binding Motif Identified in Flexible Linker Region of Pin1. While the three independently determined K_D values reported above fall within a relatively narrow range (22.4 to 27 μM), the K_D values determined using WW53 are consistently weaker than that determined using WW50. We hypothesized that this difference could be due to the three additional residues (E51-P52-A53) at the C-terminus of WW53, which are located within the flexible linker region separating the WW and PPIase domains of Pin1. Interestingly, NMR titration experiments performed using ^{15}N-WW53 in HEPES buffer (pH 6.9) at 298 K yielded broader peaks in the apo than in the ligand-saturated state, suggesting the occurrence of chemical exchange in the apo state (Figure 6A). Truncation to residue G50 (WW50) eliminated this
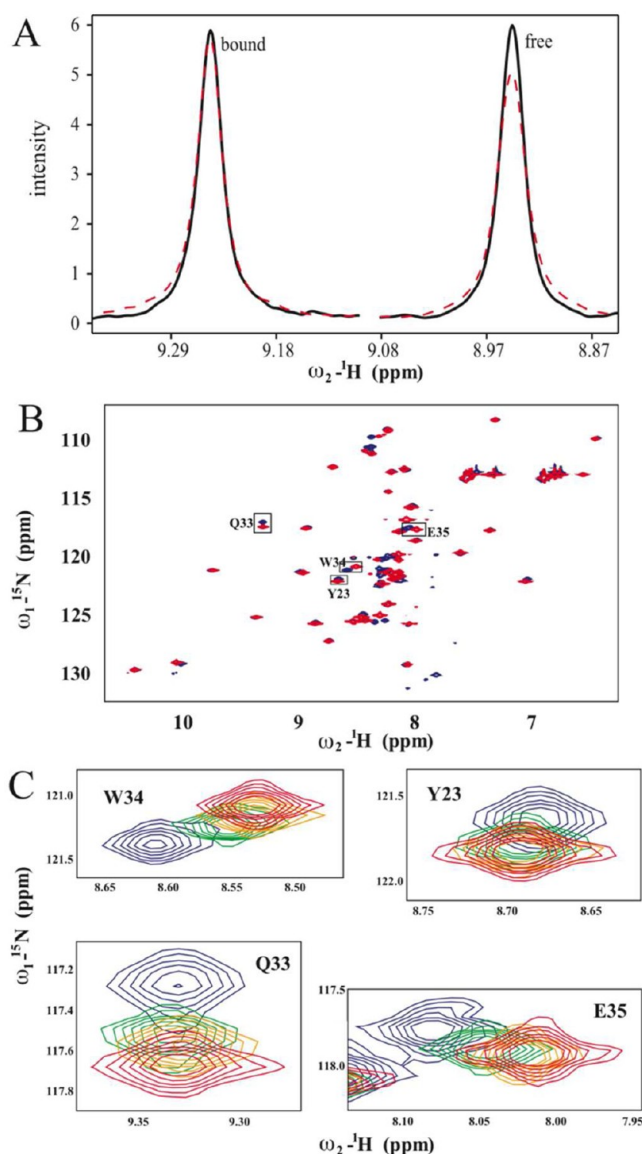
Figure 6. Detection of weak association of C-terminal WW53 residues with WW binding surface. (A) Normalized 1D slices of the backbone NH peak of S16, either in the WW50 construct (Pin1 residues 1−50, in black) or the WW53 construct (Pin1 residues 1−53, in red). For the WW53 domain saturated with pAPP659−679 (left) the line width is sharper than the apo WW53 domain (right) but in the case of WW50 the S16 line width is relatively unchanged between free and pAPP659−682 bound. (B) Overlaid HSQC spectra of WW50 (red) and WW53 (blue). The positions of the peaks of key binding surface residues (Y23, Q33, W34, E35, in boxes) shift in response to truncating the C-terminal E51-P52-A53 residues of the WW53 construct. (C) Overlaid HSQC spectra of WW53 (blue), WW53 E51A (green), WW53 E51A/P52A (orange), and WW50 (red) show progressive peak shifts for key binding surface residues, suggesting a weak interaction between the E51-P52-A53 residues and the WW binding surface.

broadening (Figure 6A) and induced chemical shift changes throughout the WW domain fold (Figure 6B), implicating E51-P52-A53 as a potential weak WW-binding sequence. Moreover, E51A and E51A/P52A mutations progressively shifted some key binding surface peaks toward their WW50 positions (Figure 6C), supporting a fast-exchange binding interaction mediated by the E51-P52-A53 region. Therefore, the slightly

weaker affinities determined by both NMR and ITC for WW53 as compared with that determined for WW50 by NMR is likely due to a weak competitive interaction with the E51-P52-A53 region in the WW53 construct. Since the WW53 concentration was significantly lower in ITC as compared to a majority of the peptide-perspective NMR titration points, the excellent agreement of the corresponding WW53 affinities suggests a concentration-independent intramolecular association of the E51-P52-A53 region with the WW binding surface. Detection of this weak interaction demonstrates the acute sensitivity of NMR line shape analysis, and illustrates the importance of identifying conditions in which the process of interest (e.g., a specific protein−ligand interaction) is isolated. Further studies are needed to ascertain whether this weak interaction has any functional role in intact Pin1.

Determination of Kinetics of Uncatalyzed pT668-P669 *cis−trans* Isomerization by Tryptophan Fluorescence. In order to complete the kinetic and thermodynamic characterization of the binding reaction scheme in Figure 3B, the uncatalyzed *cis−trans* isomerization rate of the pT668-P669 peptide bond was measured using tryptophan fluorescence. WW domain was incubated at 25 °C in a stirred cuvette until the tryptophan fluorescence signal stabilized. The pAPP659-682 peptide was then added to the cuvette and the fluorescence signal was recorded for a 10 min time course. There was an approximately 4-s delay after the peptide was added before data collection began, and during this dead time the fluorescence signal increased by a small margin, resulting from binding to the peptide initially adopting the *trans* isomer. During the subsequent time course, the signal increased further, following a single exponential curve (Figure 7). On the basis of the equilibrium *trans* and *cis* populations (93% and 7%, respectively), the relative magnitudes of the fast and slow signal increases (240 and 16, respectively) are fully consistent
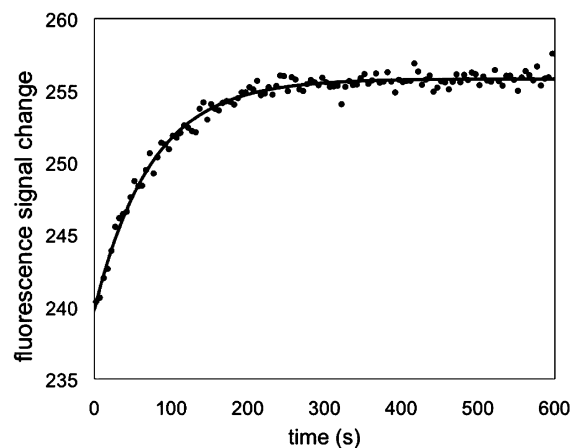

Figure 7. Measurement of kinetics of uncatalyzed pT668-P669 *cis−trans* isomerization. The time course of WW50 fluorescence intensity (arbitrary units) following mixing with pAPP659−682 peptide shows a slow increase in signal. The fluorescence signal arising from the apo WW domain was subtracted from the data to highlight the relative magnitudes of the fast and slow binding phases. The slow change in intensity reflects binding between the WW domain and newly formed *trans* isomer arising from the portion of the peptide in the *cis* conformation at the time of mixing. The rate of equilibration of binding reflects the intrinsic isomerization rates by the expression k_{obs} = k_{ct} + k_{tc}/(1 + [WW^{free}]/K_D) (see Appendix). Fitting this data yielded k_{ct} = 0.0134 s^{-1} and k_{tc} = 0.0010 s^{-1}.

with the fast signal increase resulting from the initial *trans* binding to the WW domain and the slow signal increase resulting from *cis* to *trans* conversion followed by binding. Fitting the fluorescence data to eq 12 yielded $k_{obs} = 0.0135$ s^{-1} which corresponds to $k_{ct} = 0.0134$ s^{-1} and $k_{tc} = 0.0010$ s^{-1}. These rates are in the same range as reported for other pS/T-P peptides.[57]

■ DISCUSSION

Our determination of the kinetic and thermodynamic parameters for the interaction of the WW domain with a peptide representing T668-phosphorylated APP and for the uncatalyzed *cis*−*trans* equilibrium of this peptide adds significant insight into the Pin1 reaction scheme for this biological substrate. Considering both the catalytic (PPIase) and binding (WW) domains of Pin1,[1] both of which are essential for its *in vivo* function,[15] the most general Pin1 reaction scheme involves six distinct states with eight connecting steps (Figure 8). These steps correspond to
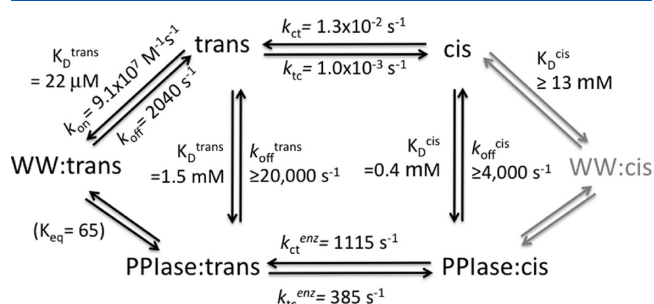

Figure 8. WW domain binding parameters placed in the context of the complete Pin1 reaction scheme. The WW domain binding parameters determined here, together with the PPIase domain binding and catalytic parameters previously reported for the same substrate in the same conditions,[41] provide a quantitative model for the complete Pin1 reaction scheme for binding to and catalysis of the pT668-P669 motif in APP. Interaction of the *cis* isomer with the WW domain (in light gray) is very weak and can be neglected.

binding, on-enzyme catalysis, or substrate transfer between the two domains. Since binding of the *cis*-isomer to the WW domain can be neglected, the Pin1 reaction scheme is reduced to five states. The substrate off-rate ($k_{off} = 2040$ s^{-1}) determined here for the isolated WW domain is roughly in the same time regime as the on-enzyme catalysis rate ($k_{ex} = k_{ct}^{enz} + k_{tc}^{enz} = 1500$ s^{-1}) determined previously for the isolated Pin1-PPIase domain.[41] These two processes (WW domain binding and on-enzyme catalysis) are potentially connected by a substrate transfer step (WW:*trans* ↔ PPIase:*trans*) in intact Pin1 (Figure 8). If it is assumed that the parameters determined for the isolated domains accurately reflect the corresponding parameters in intact Pin1, the equilibrium constant for this putative transfer step ($K_{eq} = $ [WW:*trans*]/[PPIase:*trans*]) is 65. A direct transfer of substrate between the WW domain and the PPIase domain in full-length Pin1 is supported by the recent observation of stereoselective dynamic coupling between the two domains using *cis*- and *trans*-locked inhibitor analogues,[58] and by observation of peptide-induced interdomain coupling in Pin1.[55] The kinetic synchronization of on-enzyme catalysis with substrate binding to the WW domain observed here might be important in tuning substrate specificity and/or the overall catalytic activity of the enzyme.

While the WW domain is a key element of the Pin1 reaction scheme, it is not yet known whether its purpose is simply to increase the effective concentration of substrate,[15] to facilitate direct transfer of substrate to the catalytic domain,[55] to facilitate subcellular localization[59] or some combination of these or other possibilities. However, it is clear that the WW domain is required for the *in vivo* functioning of Pin1.[15] The WW domain affinity for the pAPP659-682 Pin1 substrate determined here (∼22 μM) is nearly 2 orders of magnitude tighter than the Pin1-PPIase domain affinity for the same substrate.[41] Hence, the presence of the WW domain in Pin1 could increase the frequency of encounter between the *trans* isomer substrate and the PPIase domain. Conversely, since the WW domain binding site is structurally distinct and spatially remote from the PPIase domain catalytic site, the much higher affinity of the WW domain for the *trans* isomer also has the effect of competing with the PPIase domain for the *trans* substrate. In fact, the catalytic activity of intact Pin1 is nearly equal to that of the isolated PPIase domain for other substrates[15,60] as well as for pAPP.[41] We note that the results presented herein for the pAPP substrate, which contains a single Pin1 recognition motif, do not address the potential impact of the WW domain on Pin1 catalysis of a bivalent or multivalent substrate, where two properly spaced binding motifs in a peptide ligand have been shown to dramatically enhance Pin1 binding.[23]

The on-rate for the *trans* isomer of pAPP659-682 binding to the WW domain, k_{on}, suggests that this association rate is somewhat faster than expected for a typical diffusion controlled reaction.[61] Although Brownian motion predicts protein−ligand association rates of 10^9−10^{10} M^{-1} s^{-1}, the requirements to attain a required binding orientation and to overcome an activation energy barrier typically reduce protein complex formation rates to 10^5−10^6 M^{-1} s^{-1}.[45] Faster association rates are achieved by favorable electrostatic interactions between the binding partners[42,43] and could reflect evolutionary pressure if rapid binding provides functional advantages.[44,46] The heart of the Pin1-WW domain binding site consists of a phosphate binding pocket (S16 and R17 side chains and the backbone amide of R17) and two key aromatic residues (W34 and Y23) that pack with the proline ring of the pS/T-P recognition motif, and the bound ligand typically adopts a polyproline type II (PPII) helix conformation.[16,62] The strong positive charge presented by the phosphate binding pocket supports electrostatic steering of the phosphorylated substrate to the binding surface (Figure 9). Moreover, the preordered *trans* isomer of the pS/T-P motif of the APP substrate, the transiently structured nature of this sequence,[35,36] and the prevalent sampling of PPII helix structure by sequences that do not adopt a stable fold[63,64] are favorable for productive binding upon diffusion-mediated encounters. Thus, the intrinsic features of both the WW-domain binding surface and the pS/T-P motif in the APP cellular target are likely to contribute to the rapid association rate.

The common structural and electrostatic features of Pin1 substrates suggest that the very fast WW binding kinetics determined for pAPP are likely to be broadly representative of its interactions with other cellular substrates. This generalization is supported by the difficulties encountered in previous attempts to quantify the rapid WW binding kinetics for other ligands using SPR.[24,30] In the dynamic cellular milieu, where Pin1 has a vast number of different substrates that appear and vanish with the regulated action of proline-directed serine/ threonine kinases and phosphatases, fast binding and release of
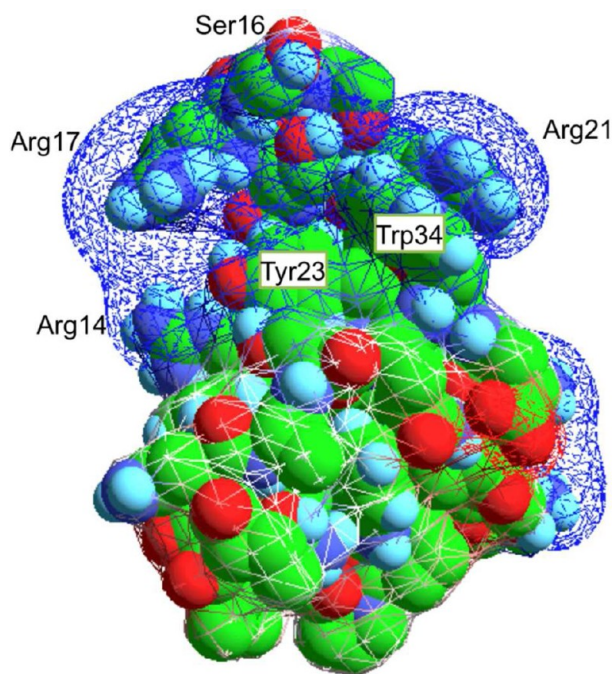
Figure 9. Electrostatic potential of Pin1-WW domain. The electrostatic potential (including partial charges) for the WW domain (X-ray structure 1f8a.pdb) was calculated within DeepView[72] using a Coulomb potential with a dielectric constant of 80 for solvent and 4 for protein, and solvent ionic strength of 0.1 M. WW domain atoms are shown as CPK-colored space-filled spheres, the electrostatic potential is mapped onto the molecular surface, and displayed using DeepView.[72]

substrates would provide key advantages. In a given cellular timing circuit regulated by Pin1, these fast kinetic features of the WW domain would allow rapid response to phosphorylation signals and to shifts in the relative populations of the multitude of Pin1 substrates.[4,5]

The studies reported here suggest that pAPP forms a relatively weak, highly transient complex with Pin1 in the cell. The K_D value (~22 μM), measured independently by the isomer-sensitive methods of NMR line shape analysis and ITC, indicates that at the much lower cellular concentrations of pAPP and Pin1, only a small fraction of pAPP will be bound to Pin1. This indicates that, in the absence of any additional factors that might contribute to a stronger ternary or higher order complex, the *trans*-specific WW domain is a minor interaction partner of pAPP in the cell. Confocal microscopy and immunostaining show that, while APP and Pin1 colocalize in certain locations, they are also largely independently distributed in the cell.[10] This transient, weak interaction is to be expected for an enzyme/substrate interaction, and suggests that the isomerase activity of Pin1, not its binding, might be the primary function influencing APP processing.

In summary, the work described here focuses on the interaction of the Pin1 WW domain with a phosphopeptide mimic of a phosphorylated form of APP that is implicated in AD. The results presented herein yield the microscopic parameters for the WW domain binding step in the multistate Pin1 reaction scheme for the APP substrate, and suggest that the synchronicity of the WW domain binding rate and the on-enzyme catalytic rate might have a functional role. The rapid binding kinetics of this interaction determined here would be advantageous for the role of Pin1 as a hub and timing device in

the multiple cellular processes in which it is known to participate.[4,5,65] These studies further highlight the powerful combination of NMR, ITC and fluorescence experiments for studying *cis-trans* isomer-specific interactions, since the coupled equilibria of binding and uncatalyzed isomerization occur on widely different time scales.

More broadly, the studies reported herein highlight NMR as a powerful and unique tool for measurement of kinetic processes that occur on time scales beyond the range of other biophysical methods. Moreover, our quantification of weak phosphate binding and weak intramolecular binding between the linker region (E51-P52) and the WW domain binding surface illustrates the sensitivity of NMR line shapes to highly transient interactions, and emphasizes the importance of establishing experimental conditions in which the specific interaction(s) of interest dominate the observed changes in line shape. These studies further underscore the ability of NMR line shape analysis to handle complex reaction schemes involving multiple states, and its suitability for study of reaction schemes where a known parameter such as ligand concentration, pH or temperature can be systematically varied.[66−68] This underutilized method significantly expands the scope, in terms of accessible time scales and reaction scheme complexity, of biophysical studies of protein kinetics and thermodynamics.

■ APPENDIX

Formalism for thermodynamic characterization of isomer-specific interactions by ITC.

To obtain the association constant (K_A) and enthalpy change (ΔH) for a binding reaction, standard equations that depend on these parameters are employed that express the binding heat evolved as a function of total concentrations of binding partners, allowing these parameters to be obtained from fitting of the binding isotherm.[69] However, when an interaction is isomer-specific these standard equations must be modified to account for the additional *cis−trans* equilibrium, including its impact on isomer concentrations and its contribution to the total heat evolved. For the *trans*-specific WW binding reaction, the total heat (q_i) of each isotherm peak 'i' corresponding to the *i*th injection of ligand has two components: heat resulting from the rapid *trans* isomer binding to the WW domain ($q_{b,i}$)[69] and heat resulting from the slow conversion of *cis* to *trans* isomer ($q_{ct,i}$):

$$q_i = q_{b,i} + q_{ct,i} \tag{A1}$$

The heat evolved due to the *trans* isomer binding to the WW domain after injection 'i' is expressed by a standard equation,[69] but with the modification that the molar concentration of free *trans* isomer after injection 'i', $[T]_i$, is required:

$$q_{b,i} = \Delta H_b \frac{K_A[T]_i}{1 + K_A[T]_i}[WW]_{tot,i}V_{cell} - \Delta H_b \frac{K_A[T]_{i-1}}{1 + K_A[T]_{i-1}}$$
$$[WW]_{tot,i-1}(V_{cell} - V_{inj}) \tag{A2}$$

where ΔH_b is the binding enthalpy per mole, $[WW]_{tot,i}$ is the total WW domain molar concentration after injection 'i', $[WW]_{tot,i-1}$ is the total WW domain molar concentration after equilibration of the previous injection 'i−1'(corrected for dilution effect by eqs A4, *vide infra*), K_A is the association constant, V_{cell} is the reaction cell volume, V_{inj} is the volume of each injection, and $[T]_{i-1}$ is the molar concentration of the free

trans isomer after equilibration of the previous injection 'i−1'. $[T]_i$ is calculated by solving the following set of equations,

$$[L]_{\text{tot},i} = [T]_i + [C]_i + [WW:T]_i \tag{A3a}$$

$$[WW]_{\text{tot},i} = [WW]_i + [WW:T]_i \tag{A3b}$$

$$K_{\text{isom}} = \frac{[T]_i}{[C]_i} \tag{A3c}$$

$$K_A = \frac{[WW:T]_i}{[WW]_i[T]_i} \tag{A3d}$$

where $[L]_{\text{tot},i}$, $[C]_i$, $[WW:T]_i$ and $[WW]_i$ are the molar concentrations of total ligand, free *cis*, bound protein and free protein, respectively, in the reaction cell after injection 'i'. During the course of the experiment, the volume of solution ejected from the reaction cell equals the volume of ligand injected, which dilutes the concentration of the protein as follows:[69]

$$[WW]_{\text{tot},i} = n[WW]_{\text{tot},0}(D)^i \tag{A4a}$$

where $[WW]_{\text{tot},0}$ is the initial WW domain molar concentration before any injection, 'n' is the stoichiometry of the binding reaction, and D (raised to the ith power) is the dilution factor given by:

$$D = \left(1 - \frac{V_{\text{inj}}}{V_{\text{cell}}}\right) \tag{A4b}$$

In eqs A2 and A3, $[WW]_{\text{tot},i}$ is scaled according to eqs A4 to account for this dilution effect.

The heat evolved as a result of the conversion of *cis* to *trans* isomer, $q_{ct,i}$, is governed by the *cis*−*trans* equilibrium constant for the free ligand, K_{isom}, and its associated enthalpy,

$$q_{ct,i} = \Delta H_{ct}\left(\frac{D[T]_{i-1}}{K_{\text{isom}}} + \frac{(1-D)[L]_{\text{tot},0}}{1 + K_{\text{isom}}} - \frac{[T]_i}{K_{\text{isom}}}\right)V_{\text{cell}} \tag{A5}$$

where ΔH_{ct} is the enthalpy per mole for conversion of *cis* to *trans*, $[L]_{\text{tot},0}$ is the molar concentration of total ligand in the syringe, and D is the dilution factor as given by eq A4b.

To determine K_A, ΔH_b, ΔH_{ct}, and n for the *trans*-specific interaction of the WW domain with ligand, the measured isotherm (heat evolved as a function of molar concentrations of binding partners) is fit to eq A1 (expressed in terms of eqs A2 and A5). The total molar concentrations, cell and injection volumes, and K_{isom} are treated as known parameters.

Derivation of exponential expression for time-dependence of slow *cis*−*trans* isomerization during fluorescence experiment.

In the fluorescence experiment, the concentration of free WW domain is approximately constant during the time course, as it is in more than 2-fold excess over the peptide (0.42 versus 0.15 mM) and the vast majority of the peptide binds within the dead time of the measurement. Therefore, WW binding is pseudo first-order during the fluorescence time course, permitting the use of an analytical expression to describe the time dependence of the concentration of the bound species. Generally, this is given by a sum of two exponentials with rate constants k_1 and k_2, given by[70,71]

$$k_1 = (A + \sqrt{A^2 - 4B})/2 \tag{A6a}$$

$$k_2 = (A - \sqrt{A^2 - 4B})/2 \tag{A6b}$$

where

$$A = k_{ct} + k_{tc} + k_{off} + k_{on}[WW^{\text{free}}] \tag{A6c}$$

$$B = k_{ct}(k_{on}[WW^{\text{free}}] + k_{off}) + k_{tc}k_{off} \tag{A6d}$$

We have shown that the first-order on and off rates of binding in the fluorescence experiment ($k_{off} = 2040$ s^{-1}, $k_{on}[WW^{\text{free}}] = 26\,000$ s^{-1}) are fast compared to typical prolyl isomerization rates, which are on the order of 0.01 s^{-1},[57] which results in $k_1 \gg k_2$ and allows for the approximations[70]

$$k_1 = k_{on}[WW^{\text{free}}] + k_{off} \tag{A7a}$$

$$k_2 = k_{ct} + k_{tc}/(1 + [WW^{\text{free}}]/K_D) \tag{A7b}$$

Since the fluorescence experiment did not make measurements during the first few seconds after mixing, during which fast binding with the rate constant k_1 goes to completion, the fluorescence time course should be defined by a single exponential with rate constant $k_{\text{obs}} = k_2$. The time-dependent fluorescence signal $I(t)$ is thus given by

$$I(t) = I_{\text{final}} + (I_0 - I_{\text{final}})e^{-tk_{\text{obs}}} \tag{A8}$$

where I_0 and I_{final} are the fluorescence intensity at the first measured point and after equilibrium has been reached, respectively.

■ ASSOCIATED CONTENT

ⓢ Supporting Information

Four supplemental figures and one supplemental table are available. Figure S1 documents the invariability of the WW domain R17 and S16 amide chemical shifts in the pH range of 5.6 to neutral. Figure S2 illustrates determination of the affinity of the WW domain for HEPES. Figure S3 illustrates the pH-dependence of amide chemical shifts for the ^{15}N-labeled peptide ligand. Figure S4 shows the quality of fit for ^{15}N-WW50 data sets used in the line shape analysis. Table S1 reports the fitting results for all residues that were quantitatively evaluated by line shape analysis. This material is available free of charge via the Internet at http://pubs.acs.org.

■ AUTHOR INFORMATION

Corresponding Author
*E-mail: lkn2@cornell.edu, phone: 607-255-7208, fax: 607-255-6249.

Present Address
#Department of Biochemistry and Molecular Biology, Department of Chemistry, and Michael Smith Laboratories, The University of British Columbia, Vancouver BC, V6T 1Z3, Canada.

Notes
The authors declare no competing financial interests.

■ ACKNOWLEDGMENTS

thank Gerald Feigenson for use of the fluorescence spectrophotometer.

ABBREVIATIONS USED

REFERENCES

(1) Ranganathan, R., Lu, K. P., Hunter, T., and Noel, J. P. (1997) Structural and functional analysis of the mitotic rotamase Pin1 suggests substrate recognition is phosphorylation dependent. *Cell 89*, 875−886.

(2) Yaffe, M. B., Schutkowski, M., Shen, M., Zhou, X. Z., Stukenberg, P. T., Rahfeld, J. U., Xu, J., Kuang, J., Kirschner, M. W., and Fischer, G. (1997) Sequence-specific and phosphorylation-dependent proline isomerization: a potential mitotic regulatory mechanism. *Science 278*, 1957.

(3) Lu, K. P., Liou, Y. C., and Zhou, X. Z. (2002) Pinning down proline-directed phosphorylation signaling. *Trends Cell Biol 12*, 164−172.

(4) Lu, K. P., and Zhou, X. Z. (2007) The prolyl isomerase PIN1: a pivotal new twist in phosphorylation signalling and disease. *Nat. Rev. Mol. Cell Biol. 8*, 904−916.

(5) Liou, Y. C., Zhou, X. Z., and Lu, K. P. (2011) Prolyl isomerase Pin1 as a molecular switch to determine the fate of phosphoproteins. *Trends Biochem. Sci. 36*, 501−514.

(6) Lu, K. P., Finn, G., Lee, T. H., and Nicholson, L. K. (2007) Prolyl cis-trans isomerization as a molecular timer. *Nat. Chem. Biol. 3*, 619−629.

(7) Takahashi, K., Uchida, C., Shin, R. W., Shimazaki, K., and Uchida, T. (2008) Prolyl isomerase, Pin1: new findings of post-translational modifications and physiological substrates in cancer, asthma and Alzheimer's disease. *Cell. Mol. Life Sci. 65*, 359−375.

(8) Lu, K. P., Suizu, F., Zhou, X. Z., Finn, G., Lam, P., and Wulf, G. (2006) Targeting carcinogenesis: a role for the prolyl isomerase Pin1? *Mol Carcinog. 45*, 397−402.

(9) Zhou, X. Z., Kops, O., Werner, A., Lu, P. J., Shen, M., Stoller, G., Kullertz, G., Stark, M., Fischer, G., and Lu, K. P. (2000) Pin1-dependent prolyl isomerization regulates dephosphorylation of Cdc25C and tau proteins. *Mol. Cell 6*, 873−883.

(10) Pastorino, L., Sun, A., Lu, P. J., Zhou, X. Z., Balastik, M., Finn, G., Wulf, G., Lim, J., Li, S. H., Li, X., Xia, W., Nicholson, L. K., and Lu, K. P. (2006) The prolyl isomerase Pin1 regulates amyloid precursor protein processing and amyloid-beta production. *Nature 440*, 528−534.

(11) Lu, K. P., Hanes, S. D., and Hunter, T. (1996) A human peptidyl-prolyl isomerase essential for regulation of mitosis. *Nature 380*, 544−547.

(12) Nicholson, L. K., and Lu, K. P. (2007) Prolyl cis-trans Isomerization as a molecular timer in Crk signaling. *Mol. Cell 25*, 483−485.

(13) Nicholson, L. K., and De, S. (2011) Structural biology: The twist in Crk signaling revealed. *Nat. Chem. Biol. 7*, 5−6.

(14) Kouri, E. D., Labrou, N. E., Garbis, S. D., Kalliampakou, K. I., Stedel, C., Dimou, M., Udvardi, M. K., Katinakis, P., and Flemetakis, E. (2009) Molecular and biochemical characterization of the parvulin-type PPIases in Lotus japonicus. *Plant Physiol. 150*, 1160−1173.

(15) Lu, P. J., Zhou, X. Z., Shen, M., and Lu, K. P. (1999) Function of WW domains as phosphoserine-or phosphothreonine-binding modules. *Science 283*, 1325.

(16) Verdecia, M. A., Bowman, M. E., Lu, K. P., Hunter, T., and Noel, J. P. (2000) Structural basis for phosphoserine-proline recognition by group IV WW domains. *Nat. Struct. Biol. 7*, 639−643.

(17) Tong, A. H., Drees, B., Nardelli, G., Bader, G. D., Brannetti, B., Castagnoli, L., Evangelista, M., Ferracuti, S., Nelson, B., Paoluzi, S., Quondam, M., Zucconi, A., Hogue, C. W., Fields, S., Boone, C., and Cesareni, G. (2002) A combined experimental and computational strategy to define protein interaction networks for peptide recognition modules. *Science 295*, 321−324.

(18) Pawson, T., and Nash, P. (2003) Assembly of cell regulatory systems through protein interaction domains. *Science 300*, 445−452.

(19) Chothia, C., Gough, J., Vogel, C., and Teichmann, S. A. (2003) Evolution of the protein repertoire. *Science 300*, 1701−1703.

(20) Pawson, T., and Scott, J. D. (1997) Signaling through scaffold, anchoring, and adaptor proteins. *Science 278*, 2075−2080.

(21) Ingham, R. J., Colwill, K., Howard, C., Dettwiler, S., Lim, C. S., Yu, J., Hersi, K., Raaijmakers, J., Gish, G., Mbamalu, G., Taylor, L., Yeung, B., Vassilovski, G., Amin, M., Chen, F., Matskova, L., Winberg, G., Ernberg, I., Linding, R., O'Donnell, P., Starostine, A., Keller, W., Metalnikov, P., Stark, C., and Pawson, T. (2005) WW domains provide a platform for the assembly of multiprotein networks. *Mol. Cell. Biol. 25*, 7092−7106.

(22) Daum, S., Fanghanel, J., Wildemann, D., and Schiene-Fischer, C. (2006) Thermodynamics of phosphopeptide binding to the human peptidyl prolyl cis/trans isomerase Pin1. *Biochemistry 45*, 12125−12135.

(23) Daum, S., Lucke, C., Wildemann, D., and Schiene-Fischer, C. (2007) On the benefit of bivalency in peptide ligand/pin1 interactions. *J. Mol. Biol. 374*, 147−161.

(24) Kato, Y., Ito, M., Kawai, K., Nagata, K., and Tanokura, M. (2002) Determinants of ligand specificity in groups I and IV WW domains as studied by surface plasmon resonance and model building. *J. Biol. Chem. 277*, 10173−10177.

(25) Kato, Y., Nagata, K., Takahashi, M., Lian, L., Herrero, J. J., Sudol, M., and Tanokura, M. (2004) Common mechanism of ligand recognition by group II/III WW domains: redefining their functional classification. *J. Biol. Chem. 279*, 31833−31841.

(26) Peng, T., Zintsmaster, J. S., Namanja, A. T., and Peng, J. W. (2007) Sequence-specific dynamics modulate recognition specificity in WW domains. *Nat. Struct. Mol. Biol. 14*, 325−331.

(27) Smet, C., Duckert, J. F., Wieruszeski, J. M., Landrieu, I., Buee, L., Lippens, G., and Deprez, B. (2005) Control of protein-protein interactions: structure-based discovery of low molecular weight inhibitors of the interactions between Pin1 WW domain and phosphopeptides. *J. Med. Chem. 48*, 4815−4823.

(28) Smet, C., Wieruszeski, J. M., Buee, L., Landrieu, I., and Lippens, G. (2005) Regulation of Pin1 peptidyl-prolyl cis/trans isomerase activity by its WW binding module on a multi-phosphorylated peptide of Tau protein. *FEBS Lett. 579*, 4159−4164.

(29) Wintjens, R., Wieruszeski, J. M., Drobecq, H., Rousselot-Pailley, P., Buee, L., Lippens, G., and Landrieu, I. (2001) 1H NMR study on the binding of Pin1 Trp-Trp domain with phosphothreonine peptides. *J. Biol. Chem. 276*, 25150−25156.

(30) Fotia, A. B., Dinudom, A., Shearwin, K. E., Koch, J. P., Korbmacher, C., Cook, D. I., and Kumar, S. (2003) The role of individual Nedd4−2 (KIAA0439) WW domains in binding and regulating epithelial sodium channels. *FASEB J. 17*, 70−72.

(31) Myszka, D. G. (1997) Kinetic analysis of macromolecular interactions using surface plasmon resonance biosensors. *Curr. Opin. Biotechnol. 8*, 50−57.

(32) Madeo, J., Mihajlovic, M., Lazaridis, T., and Gunner, M. R. (2011) Slow dissociation of a charged ligand: analysis of the primary quinone Q(A) site of photosynthetic bacterial reaction centers. *J. Am. Chem. Soc. 133*, 17375−17385.

(33) Schreiber, G., Haran, G., and Zhou, H. X. (2009) Fundamental aspects of protein-protein association kinetics. *Chem. Rev. 109*, 839−860.

(34) Pastorino, L., Ma, S. L., Balastik, M., Huang, P., Pandya, D., Nicholson, L. K., and Lu, K. P. (2012) Alzheimer's disease-related loss of Pin1 function influences the intracellular localization and the processing of AβPP. *J. Alzheimer's Dis. 30*, 277−297.

(35) Ramelot, T. A., Gentile, L. N., and Nicholson, L. K. (2000) Transient structure of the amyloid precursor protein cytoplasmic tail indicates preordering of structure for binding to cytosolic factors. *Biochemistry 39*, 2714–2725.

(36) Ramelot, T. A., and Nicholson, L. K. (2001) Phosphorylation-induced structural changes in the amyloid precursor protein cytoplasmic tail detected by NMR. *J. Mol. Biol. 307*, 871–884.

(37) Li, S., Shankar, G. M., and Selkoe, D. J. (2010) How do Soluble Oligomers of Amyloid beta-protein Impair Hippocampal Synaptic Plasticity? *Front. Cell Neurosci. 4*, 5.

(38) Lee, M. S., Kao, S. C., Lemere, C. A., Xia, W., Tseng, H. C., Zhou, Y., Neve, R., Ahlijanian, M. K., and Tsai, L. H. (2003) APP processing is regulated by cytoplasmic phosphorylation. *J. Cell Biol. 163*, 83–95.

(39) Cruz, J. C., Kim, D., Moy, L. Y., Dobbin, M. M., Sun, X., Bronson, R. T., and Tsai, L. H. (2006) p25/cyclin-dependent kinase 5 induces production and intraneuronal accumulation of amyloid beta in vivo. *J. Neurosci. 26*, 10536–10541.

(40) Leroy, K., Boutajangout, A., Authelet, M., Woodgett, J. R., Anderton, B. H., and Brion, J. P. (2002) The active form of glycogen synthase kinase-3ß is associated with granulovacuolar degeneration in neurons in Alzheimer's disease. *Acta Neuropathol. 103*, 91–99.

(41) Greenwood, A. I., Rogals, M. J., De, S., Lu, K. P., Kovrigin, E. L., and Nicholson, L. K. (2011) Complete determination of the Pin1 catalytic domain thermodynamic cycle by NMR lineshape analysis. *J. Biomol. NMR 51*, 21–34.

(42) Berg, O. G., and von Hippel, P. H. (1985) Diffusion-controlled macromolecular interactions. *Annu. Rev. Biophys. Biophys. Chem. 14*, 131–160.

(43) Eigen, M., and Hammes, G. G. (1963) Elementary Steps in Enzyme Reactions (as Studied by Relaxation Spectrometry). *Adv. Enzymol. Relat. Areas Mol. Biol. 25*, 1–38.

(44) Schreiber, G., Buckle, A. M., and Fersht, A. R. (1994) Stability and function: two constraints in the evolution of barstar and other proteins. *Structure 2*, 945–951.

(45) Selzer, T., and Schreiber, G. (1999) Predicting the rate enhancement of protein complex formation from the electrostatic energy of interaction. *J. Mol. Biol. 287*, 409–419.

(46) Sydor, J. R., Engelhard, M., Wittinghofer, A., Goody, R. S., and Herrmann, C. (1998) Transient kinetic studies on the interaction of Ras and the Ras-binding domain of c-Raf-1 reveal rapid equilibration of the complex. *Biochemistry 37*, 14292–14299.

(47) Kovrigin, E. L. (2012) NMR line shapes and multi-state binding equilibria. *J. Biomol. NMR 53*, 257–270.

(48) Kaplan, J. I., Fraenkel, G. (1980) *NMR of Chemically Exchanging Systems*, Academic Press, USA.

(49) McConnell, H. M. (1958) Reaction rates by nuclear magnetic resonance. *J. Chem. Phys. 28*, 430.

(50) Liu, F., Du, D., Fuller, A. A., Davoren, J. E., Wipf, P., Kelly, J. W., and Gruebele, M. (2008) An experimental survey of the transition between two-state and downhill protein folding scenarios. *Proc. Natl. Acad. Sci. U. S. A. 105*, 2369–2374.

(51) Kowalski, J. A., Liu, K., and Kelly, J. W. (2002) NMR solution structure of the isolated Apo Pin1 WW domain: comparison to the x-ray crystal structures of Pin1. *Biopolymers 63*, 111–121.

(52) Sorrentino, G., Mioni, M., Giorgi, C., Ruggeri, N., Pinton, P., Moll, U., Mantovani, F., Del Sal, G. (2012) The prolyl-isomerase Pin1 activates the mitochondrial death program of p53, *Cell Death Differ.*

(53) Sultana, R., Boyd-Kimball, D., Poon, H. F., Cai, J., Pierce, W. M., Klein, J. B., Markesbery, W. R., Zhou, X. Z., Lu, K. P., and Butterfield, D. A. (2006) Oxidative modification and down-regulation of Pin1 in Alzheimer's disease hippocampus: A redox proteomics analysis. *Neurobiol. Aging 27*, 918–925.

(54) Zhang, Y., Daum, S., Wildemann, D., Zhou, X. Z., Verdecia, M. A., Bowman, M. E., Lucke, C., Hunter, T., Lu, K. P., Fischer, G., and Noel, J. P. (2007) Structural basis for high-affinity peptide inhibition of human Pin1. *ACS Chem. Biol. 2*, 320–328.

(55) Jacobs, D. M., Saxena, K., Vogtherr, M., Bernado, P., Pons, M., and Fiebig, K. M. (2003) Peptide binding induces large scale changes in inter-domain mobility in human Pin1. *J. Biol. Chem. 278*, 26174–26182.

(56) Burnouf, D., Ennifar, E., Guedich, S., Puffer, B., Hoffmann, G., Bec, G., Disdier, F., Baltzinger, M., and Dumas, P. (2012) kinITC: a new method for obtaining joint thermodynamic and kinetic data by isothermal titration calorimetry. *J. Am. Chem. Soc. 134*, 559–565.

(57) Schutkowski, M., Bernhardt, A., Zhou, X. Z., Shen, M., Reimer, U., Rahfeld, J. U., Lu, K. P., and Fischer, G. (1998) Role of phosphorylation in determining the backbone dynamics of the serine/threonine-proline motif and Pin1 substrate recognition. *Biochemistry 37*, 5566–5575.

(58) Namanja, A. T., Wang, X. J., Xu, B., Mercedes-Camacho, A. Y., Wilson, K. A., Etzkorn, F. A., and Peng, J. W. (2011) Stereospecific gating of functional motions in Pin1. *Proc. Natl. Acad. Sci. U. S. A. 108*, 12289–12294.

(59) Lu, P. J., Zhou, X. Z., Liou, Y. C., Noel, J. P., and Lu, K. P. (2002) Critical role of WW domain phosphorylation in regulating phosphoserine binding activity and Pin1 function. *J. Biol. Chem. 277*, 2381.

(60) Rippmann, J. F., Hobbie, S., Daiber, C., Guilliard, B., Bauer, M., Birk, J., Nar, H., Garin-Chesa, P., Rettig, W. J., and Schnapp, A. (2000) Phosphorylation-dependent proline isomerization catalyzed by Pin1 is essential for tumor cell survival and entry into mitosis. *Cell Growth Differ. 11*, 409–416.

(61) Schreiber, G. (2002) Kinetic studies of protein-protein interactions. *Curr. Opin. Struct. Biol. 12*, 41–47.

(62) Bielska, A. A., and Zondlo, N. J. (2006) Hyperphosphorylation of tau induces local polyproline II helix. *Biochemistry 45*, 5527–5537.

(63) Shi, Z., Woody, R. W., and Kallenbach, N. R. (2002) Is polyproline II a major backbone conformation in unfolded proteins? *Adv. Protein Chem. 62*, 163–240.

(64) Rucker, A. L., and Creamer, T. P. (2002) Polyproline II helical structure in protein unfolded states: lysine peptides revisited. *Protein Sci. 11*, 980–985.

(65) Tun-Kyi, A., Finn, G., Greenwood, A., Nowak, M., Lee, T. H., Asara, J. M., Tsokos, G. C., Fitzgerald, K., Israel, E., Li, X., Exley, M., Nicholson, L. K., and Lu, K. P. (2011) Essential role for the prolyl isomerase Pin1 in Toll-like receptor signaling and type I interferon-mediated immunity. *Nat. Immunol. 12*, 733–741.

(66) Kern, D., Kern, G., Scherer, G., Fischer, G., and Drakenberg, T. (1995) Kinetic analysis of cyclophilin-catalyzed prolyl cis/trans isomerization by dynamic NMR spectroscopy. *Biochemistry 34*, 13594–13602.

(67) Gunther, U. L., and Schaffhausen, B. (2002) NMRKIN: simulating line shapes from two-dimensional spectra of proteins upon ligand binding. *J. Biomol. NMR 22*, 201–209.

(68) Kovrigin, E. L., and Loria, J. P. (2006) Enzyme dynamics along the reaction coordinate: critical role of a conserved residue. *Biochemistry 45*, 2636–2647.

(69) Lewis, E. A., Murphy, K. P. (2005) *Protein-Ligand Interactions: Methods and Applications*, Humana Press Inc., New York.

(70) Ng, K. K., and Weis, W. I. (1998) Coupling of prolyl peptide bond isomerization and Ca2+ binding in a C-type mannose-binding protein. *Biochemistry 37*, 17977–17989.

(71) Hagerman, P. J., and Baldwin, R. L. (1976) A quantitative treatment of the kinetics of the folding transition of ribonuclease A. *Biochemistry 15*, 1462–1473.

(72) Guex, N., and Peitsch, M. C. (1997) SWISS-MODEL and the Swiss-PdbViewer: an environment for comparative protein modeling. *Electrophoresis 18*, 2714–2723.

■ NOTE ADDED AFTER ASAP PUBLICATION

This manuscript published ASAP on October 16, 2012. The caption of Figure 3 was modified and the revised version was reposted on October 18, 2012.